Hindawi
Advances in Civil Engineering
Volume 2021, Article ID 8847500, 11 pages
https://doi.org/10.1155/2021/8847500

Research Article

Investigation of Pressure Relief Borehole Effects Using In Situ Testing Based on Distributed Optical Fibre Sensing Technology

Yunpeng Li,[1,2,3] **Dequan Sun**,[2,4] **Shankun Zhao**,[3] **Kaihua Liang**,[2,4] **Kai Cui**,[2,4] **and Huaihong Wang**[2,4]

[1]*China Coal Research Institute (CCRI), Beijing 100013, China*
[2]*Engineering Laboratory of Deep Mine Rockburst Disaster Assessment, Jinan 250100, China*
[3]*Mine Safety Technology Branch, China Coal Research Institute (CCTEG), Beijing 100013, China*
[4]*Shandong Province Research Institute of Coal Geology Planning and Exploration, Jinan 250100, China*

Correspondence should be addressed to Shankun Zhao; zhaoshankuncom@163.com

Received 12 August 2020; Revised 15 December 2020; Accepted 26 December 2020; Published 13 January 2021

Academic Editor: Fengqiang Gong

Borehole pressure relief method is one of the most effective ways of rock burst prevention in coal mines. The measured results of borehole pressure relief at no. 8939 longwall face in Xinzhouyao coal mine, China, are presented here. The analyses identify the pressure relief magnitudes in coal mass around the boreholes with different diameters, spacing, and drilling time. This research has established that the best pressure relief of the rib coal can be achieved by using φ108 mm borehole with 0.7 m interval after 288 hours. The strain relief is acceptable after 288–360 hours of drilling, while the best result is achieved after 432 hours. It is also the first time to monitor the borehole pressure relief in a coal mine on-site using Brillouin optical time domain reflectometer (BOTDR) distributed fibre-optic sensing. The method implemented in this research provides new ways to improve stress relief design and minimize the rock burst occurrence for mine practitioners.

1. Introduction

Rock burst is a complex dynamic phenomenon of rock failure in highly stressed ground. Its destructive power is a major safety hazard in deep coal mines. Prediction of rock bursts is extremely difficult. One key to minimize the rock burst occurrence is the reduction of stress within the ground. Based on engineering empirical, the pressure relief borehole method is one of the most successful and commonly used ground stress relief methods. When the drilling bits close to the highly stressed area, the frequency and intensity of small coal bursts surrounding the boreholes increase. Highly stressed area accumulates more potential energy resulting in high burst proneness. Thus, the boreholes drilled within highly stressed coal can fracture and soften the surrounding coal mass effectively [1, 2]. Theoretical analysis, numerical calculation, and electromagnetic radiometer can be used to determine the yielded zone. However, the investigation of the development of the yielded zone lacks field testing.

Feasibility studies have therefore been performed using experiments on both models and actual structures. At present, the commonly used methods to predict strata failure include [3–11] empirical formulas, physical modelling, numerical simulations, field observations, microseismic system, etc. However, they also have defects in practice. For example, by using theoretical analysis, the coal body around the borehole can be assumed as the Mohr-Coulomb material. This calculated fracture zone around the borehole is acceptable, but it can hardly estimate the crack zone. One empirical coefficient is introduced to calculate the fracture zone, but the coefficient is highly empirical should be considered case by case. Similarly, the numerical methods can hardly simulate the collapse and compaction processes after the coal body broken. The current in situ monitoring methods are mainly using microseismic monitoring and in situ observation. The allowable error of the microseismic monitoring is about 10 m, while the radius of one pressure relief borehole is about 1 m. Observation of the borehole can

only reach 1~2 m from the hole collar, and engineering judgment is highly relied on past experiences [12]. In summary, current methods estimate the deformation of coal indirectly. Accordingly, a technology capable of monitoring the deformation of the coal directly is highly desirable. Distributed optical fibre sensing technology is a new strain monitoring technology, which can be implanted into the coal mass to monitor the deformation of the coupling coal body.

Distributed optical fibre sensing technologies (DOFS), including optical time-domain reflectometry (OTDR) [13], Brillouin optical time-domain analysis (BOTDA) [14], Brillouin optical time-domain reflectometry (BOTDR) [15], and Brillouin optical frequency-domain analysis (BOFDA) [16], have developed rapidly over the past decade. Recently, BOTDRs are expected to be used for structural monitoring and diagnosis via measuring strain accurately and continuously over dozens kilometers using only one end of an optical fibre. Nan and Gao [17] constructed the physical and mechanical models using distributed optical fibre based on BOTDR to study one section of Si Jiaying iron mine in China, and BOTDR showed advantages such as distributiveness, precision, easy arrange, and good anti-interference. Xu et al. [18] measured the sinkhole collapse strain using the distributed Brillouin optical fibre sensor. Based on the time-series data, an AR(2) sinkhole collapse model was constructed. Suo et al. [19] used the distributed fibre-optic sensing (DFOS) to monitor ground fissures in complicated field. A fixed-point fibre-optic sensing cable (FFOSC) was designed, and the corresponding installation method was developed. Results show that the FFOSC provides a solid basis for the investigation of ground fissure mechanisms. Moffat et al. [20] made a strain monitoring system based on a PVC tube instrumented with an optical fibre connected to a Brillouin optical time domain reflectometer (BOTDR) apparatus. Four lines of optical fibre are glued along the tube surface, which are rotated 90° one from each other, to capture in-plane and out-of-plane tube bending displacements. The conclusions of the study suggest that the proposed sensor can be regarded as a promising and safe tool for tunnel monitoring. Madjdabadia et al. [21] built unique distributed Brillouin sensing systems (DBSs) to determine the deformational behaviour of excavations in underground mining. The filling thickness and strength were studied based on the strain measurement using a larger diameter beam and weaker strength beam, respectively. In both tests, DiTeSt™ showed the same performance as with a smaller beam and stronger mortar. Pulse-prepump Brillouin optical time domain analysis (PPP-BOTDA) is a novel technique for distributed strain measurements. Guo et al. [22] used it to measure the bond strength of the steel rebars and bending moment of the concrete girders. Results show that the PPP-BOTDA provides a precise description of the strain distribution of the rebar and the concrete, exhibiting the ability for crack detection. Klar et al. [23] also present this technology for monitoring ground displacement using the analysis of signal derived from a horizontally laid fibre above the tunnel. The Brillouin optical time domain reflectometry/analysis (BOTDR/A) and Rayleigh backscatter wavelength interferometry (OBR) were compared, and the results obtained by different technologies showed that both of them were equally suitable for the suggested approach. Distributed optical fibre sensors (DOFS) have been attracting significant attention by geotechnical engineering community. Innovative structural design, encapsulation development, and implementation methods of optical fibre sensors lead to new applications in the geotechnical monitoring. Recent application of using two successful technologies includes Brillouin optical time domain reflectometry (BOTDR) and Brillouin optical time domain analysis (BOTDA) for geotechnical monitoring, such as geotextiles, soil nails, anchors, pipelines, retaining walls, tunnels, and landslides [24]. This suggests that BOTDR technology with a single-ended input is suitable for the underground coal mining.

In this paper, a site application has been realized to investigate the process of borehole pressure relief using BOTDR. A specially designed BOTDR sensing fibre was developed and buried into the coal seam to measure the internal strain distribution after the pressure relief boreholes were constructed. The monitoring results have been analyzed in detail, including the relationship between the pressure relief and the duration, location, and size of the borehole.

2. BOTDR Sensing Technology for Pressure Relief Borehole

2.1. Working Principle of BOTDR Sensing Technology. The light waves in optical fibre travel in straight lines mostly. However, due to the existence of uneven structures of noncrystalline materials in microdimension, a small fraction of light will produce scattering. Brillouin scattering is one of the light scattering types in optical fibres, which is caused by acoustic phonons. The basic principle of BOTDR is using the linear relationships between the frequency shift variation of the natural fibre distribution Brillouin scattering light. The schematics of strain measurement using the BOTDR is shown in Figure 1. The Brillouin frequency shift of the scattered light generated inside a single-mode optical fibre has an axial linear relationship with the applied strain and temperature, regardless of the temperature change, and it can be expressed by [3]

$$\upsilon_B(\varepsilon) = \upsilon_B(0) + \frac{d\upsilon_B(\varepsilon)}{d\varepsilon} \times \varepsilon. \quad (1)$$

where $\upsilon_B(\varepsilon)$ is the drift quantity of Brillouin scattering light frequency when the optical fibre strain occurs; $\upsilon_B(0)$ is the drift quantity of Brillouin scattering light frequency without strain in the optical fibre; $d\upsilon_B(\varepsilon)/d\varepsilon$ is the scale factor; ε is the fibre axial strain.

The optical fibre used in BOTDR sensing technology is small, so the optical fibre can be embedded in the coal seam to conduct distributed measurement with nearly no effect on the structure. For the whole optical fibre, the measured variable is wavelength; therefore, joint loss and light pathway loss have a little influence on the optical fibre; the environmental interference is not sensitive.

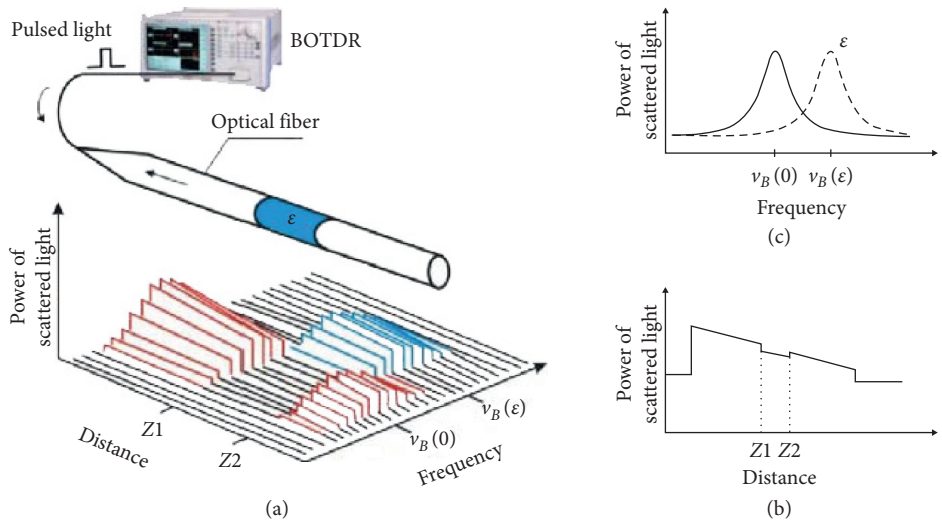

Figure 1: Schematics of strain measurements with BOTDR.

2.2. Borehole Pressure Relief Model Based on BOTDR. The coal mass around the pressure relief borehole breaks gradually, and the crushed coal collapses into the borehole. This process leads to stress redistributing around the borehole, causing the range of yielded zone to increase. Finally, the free space is filled with crushed coal mass. Thereby, a pressure relief area is formed by rupture zone, plastic zone, and elastic zone [12]. To analyze the deformation of the coal mass around a pressure relief borehole, a borehole pressure relief model under plane stress state is established, as shown in Figure 2.

The optical fibre and the pressure relief borehole are arranged crosswise. When the coal mass surrounding a pressure relief borehole produces a radial displacement, the optical fibre generates an axial strain due to optical fibre cable bending. Under the action of the vertical stress, the optical fibre cable sensor moves downward, vertical displacement is Δh, and the length of the optical fibre that produces tensile deformation is L, and the geometric relationship is as follows:

$$R = \sqrt{h^2 + \left(\frac{L}{2}\right)^2}. \quad (2)$$

where R is the yielded zone radius; h is the distance between the optical fibre and the center pressure relief borehole; L is the length of the optical fibre that produces tensile deformation.

The middle section of the optical fibre is in tension, and its bending moment is positive. The vicinity sections of two ends are under compression, and their bending moments are negative. Therefore, when the strain of the optical fibre is below zero, it is the boundary of the pressure relief areas.

2.3. Borehole Pressure Relief Model Numerical Simulation. FLAC^{3D} was used to establish the model shown in Figure 2. The length, width, and height of the model were 1 m, 10 m, and 1 m, respectively. A total of 800,000 zones and 848,421 nodes were established. In the model, cable structural element is used to simulate the strain of the sensor optical cable. One unit cable element is 0.1 m in length. Models using Mohr-Coulomb criterion and the mechanical parameters of the model are shown in Table 1.

The model boundary conditions are as follows:

(1) The boundary at both ends of the X-axis of the model is restricted along the X-axis; that is, the displacement of the boundary in the X direction is zero

(2) The boundary at both ends of the Y-axis of the model is restricted along the Y-axis; that is, the displacement of the boundary in the Y direction is zero

(3) The bottom boundary of the model is fixed; that is, the displacement of the bottom boundary in the X, Y, and Z directions is zero

(4) The top of the model is a free boundary

In situ stress conditions are as follows:

(1) A gradient stress of 8.18 MPa~6.35 MPa is applied in the X-axis direction of the model

(2) A gradient stress of 13.40 MPa~10.40 MPa is applied in the Y-axis direction of the model

(3) Apply a gradient stress of 9.45~7.33 MPa in the Z axis direction of the model

(4) The upper rock layer of the model is simulated by applying an equivalent load, and its value is 6.23 MPa

After the model is initially balanced, a borehole with 108 mm diameter and 10 m depth was drilled, and the large deformation mode is used for calculation. After the model is balanced, the cable structural element strain curve is shown in Figure 3.

It can be seen from Figure 3 that after the borehole was drilled, the sensing fibre was deformed, which was consistent with the expected pattern of the theoretical analysis. The feasibility of this method for in situ testing of pressure relief boreholes is verified.

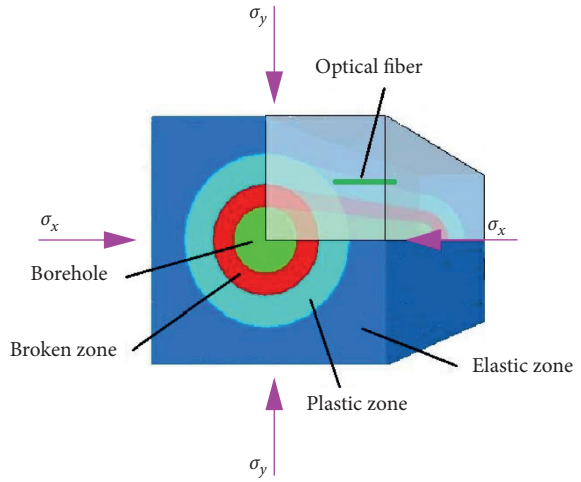

Figure 2: Geometric model of borehole pressure relief.

Table 1: Numerical model mechanical parameters.

Types	Density (kN·m^{-3})	UCS (MPa)	UTS (MPa)	Young's modulus (GPa)	Poisson's ratio	Cohesion (MPa)	Friction angle (°)
Coal	1293	32.27	1.34	3.66	0.20	3.67	29.89
Types	Density (kN·m^{-3})		Young's modulus (GPa)	Grout cohesion (MPa)	Grout friction angle (°)	Cross-sectional area (mm^2)	Tensile yield strength (N)
Cable	2660		3.80	3.00	25.00	19.63	2350

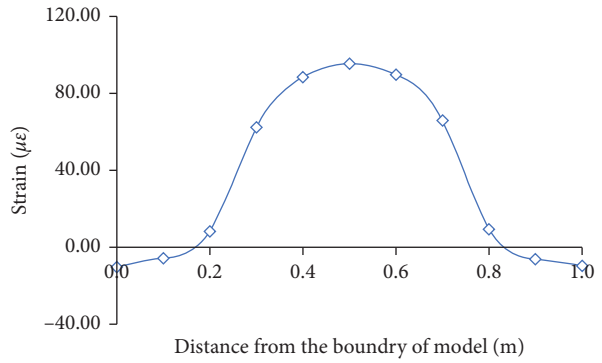

Figure 3: Numerical simulation of optical fibre strain curve.

3. Engineering Background

Xinzhouyao coal mine is located in Datong, Shanxi, China. Datong coalfield is a syncline structure basin located in an axial direction from northeast to south-west. Its east boundary is Kouquan fault which is adjacent to the new belt graben basin (Datong plain); the west boundary is Xishi Mountains in Lvliang meridional tectonic belt; the south takes the east-west small Hongtao Mountain anticline as the boundary, and the south is linked to Pingshuo and Ningwu coalfield. Datong mining area is a typical dual comining area (Jurassic system and Permo-Carboniferous system). Xinzhouyao coal mine is located in the northeast of Datong coalfield, belonging to the synclinal east wing of Datong, and mining Jurassic 9#, 11#, 12#, and 14# coal seams. The basic structure form of this mine field is the northeast 10°~50° in monoclinal structure with the tendency to the northwest, high in the east and low in the west, adjacent to the west side of the Kouquan fault.

No. 8939 longwall panel in Xinzhouyao coal mine is at the eastern mine boundary. The remnant triangular pillar after mining is located between the longwall panel and the adjacent no. 8941 panel. The main roadways in no. 903 panel consist of the main haulage roadway and rail roadway, and the main ventilation roadway all located south of no. 8939 longwall panel. West of no. 8939 longwall panel is the old goaf of no. 8937 panel. North of no. 8939 longwall panel is the protection coal pillar forming the mine boundary (adjacent to the Yungang coal mine), so no. 8939 panel is a typical island mining panel.

No. 11 coal seam in no. 8939 panel is mined using the comprehensive mechanized cover caving method (top coal caving method). The average thickness of the coal seam in no. 8939 panel is 7.2 m, the average inclination is 3°, the gas emission is 4.7 m^3/min, and the coal seam hardness is 3.2. The coal cutting height is 3 m, while the coal caving height is 4.2 m, giving the ratio of cutting to caving 1 : 1.4. The direct roof of the coal seam is siltstone and fine sandstone with a thickness of 2.1 m~3.3 m, the main roof is medium and fine sandstone with a thickness of 14.0 m~17.5 m, and the floor is siltstone with a thickness of 1.68 m~5.02 m. Roof management is combined with the natural collapse method and blasting roof caving method. The longwall panel length is 1227.8 m, while the panel width is 94.5 m. The panel layout consists of four roadways located at various levels above the base of the 7.2 m thick coal seam. The longwall main gate and the tailgate were driven along the floor, while the middle roadway and second tailgate roof levels are located at the seam top. The position of the panel is shown in Figures 4 and 5.

The numerical simulation indicated that vertical stress would increase significantly around the barrier coal pillar and triangle pillar located between nos. 8937 and 8941 panels. The model indicated that, in the excavation process of the four roadways, the vertical stress redistributing area reaches 80 m far, and the maximum vertical stress is 23 MPa, 10 m in front of the working face. When mining the triangular pillar, the peak stress reached 27.4 MPa with the stress concentration factor of 3.8.

Originally, one row of boreholes was drilled in no. 5939 tailgate. The diameter of the boreholes drilled into coal pillar was 108 mm with 0.5 m spacing, depth of 8 m, and drilling height of 0.8 m to 1.0 m above the floor. The boreholes were perpendicular to the roadway rib. Then, the borehole length was enlengthened to 12 m to meet the requirements of the coal mine safety authority. It is necessary to further optimize the borehole pressure relief. This study analyzes the time-dependent stress relief of the boreholes under different diameters, lengths, spacings, and distance from the working space, to provide a technical support for rock burst prevention.

4. Distributed Optical Fibre Monitoring Program

4.1. The Objective of Distributed Optical Fibre Monitoring. No. 8939 longwall panel in the west wing of the mine syncline was chosen as the monitoring area. The optical fibre monitoring equipment was used to monitor the borehole pressure relief. The effect of borehole pressure relief is reflected by the strain change measured using the optical fibre equipment after drilling and provide the basis for optimising the parameters to minimize rock burst occurrences. The effect of drilled holes with different diameters, borehole interval, and ground pressure change upon time is studied.

The monitoring hole of the distributed optical fibre was drilled from the winch room in no. 5939 tailgate roadway. The monitoring borehole parameters were as follows: the distance from the rib side was 1.4 m; the height from the floor was 1.2 m; the included angle between the monitoring hole and roadway was 5°; the horizontal elevation was 1°; borehole diameter was 65 mm; borehole depth was 44 m, as shown in Figure 6.

4.2. Sensing Optical Cable and Installation. Taking into consideration the field conditions, the sensors used in this research were strain sensing cable fixed by steel wire. The diameter of the sensing cable is 5 mm ± 0.2 mm, its gauge factor is 499.8 MHz/%, the maximum breaking force is 2.35 kN, and Young's modulus is 3.80 GPa. The structure of the optical cable is shown in Figure 7.

After the optical fibre hole was drilled, the sensing cable was implanted into the hole with a 40 mm diameter PVC pipe, as shown in Figure 8. Then, the borehole collar was sealed, and the hole was filled with cementitious grout, so that the sensor cables can be bonded with surrounding rock, as shown in Figures 9 and 10. After connecting between the sensing optical cable and communication cable, the cable was attached to the air tube hanging along the roadway side and brought to the main roadway, where it was connected to the BOTDR data acquisition instrument, as shown in Figure 11.

4.3. Arrangement of Pressure Relief Borehole. Total 21 pressure relief boreholes were drilled within 44 m along the tailgate. To investigate the relationship between borehole diameter and pressure relief, three borehole diameters of 108 mm, 90 mm, and 65 mm were selected. To study the influence of borehole spacing, a group of twelve 108 mm diameter boreholes were drilled at intervals of 0.5 m, 0.6 m, 0.7 m, 0.8 m, 0.9 m, and 1.0 m. The distance between each monitored task was 1.5 m.

Boreholes numbered 7#, 10#, and 11# were used to investigate the time domain stress relief around the monitored boreholes. Before testing, two pilot holes were drilled at about 40 m from the wench room. Sudden strain changes of the optical fibre cable were detected, which shows that the optical fibre position is consistent with the design. The layout of pressure relief borehole is shown in Figure 12.

4.4. Data Collection and Analysis. After the grout cured, the initial strain distribution of the sensing optical cable was recorded. The strain distribution of the optical cable in borehole was then monitored periodically. The strain changes adjacent to all boreholes were measured by the optical fibre cable including the time-dependent stress relief. BOTDR distributed optical fibre sensing technology is single-ended testing. Only one end of the sensing optical

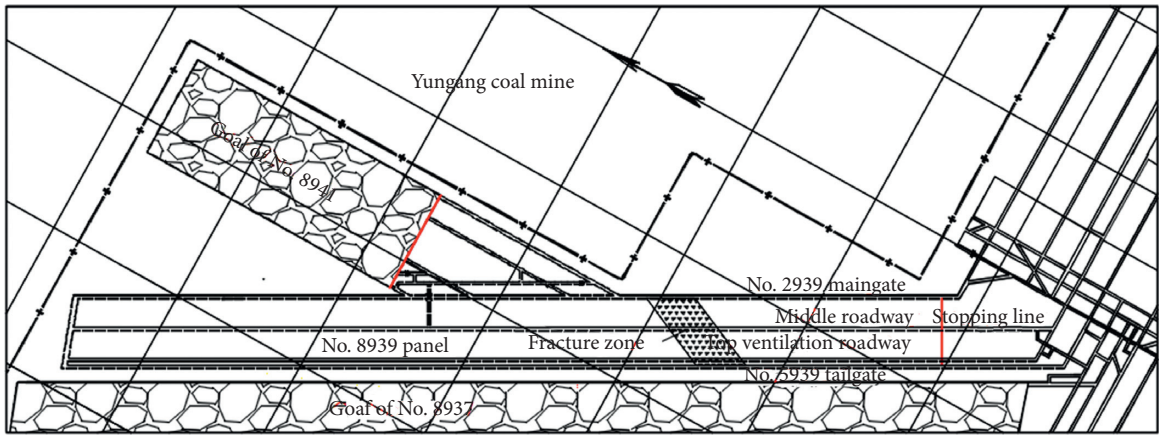

Figure 4: Plan view of no. 8939 longwall panel.

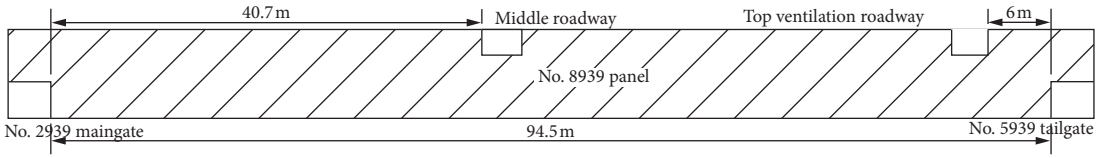

Figure 5: Roadway layout of no. 8939 longwall panel.

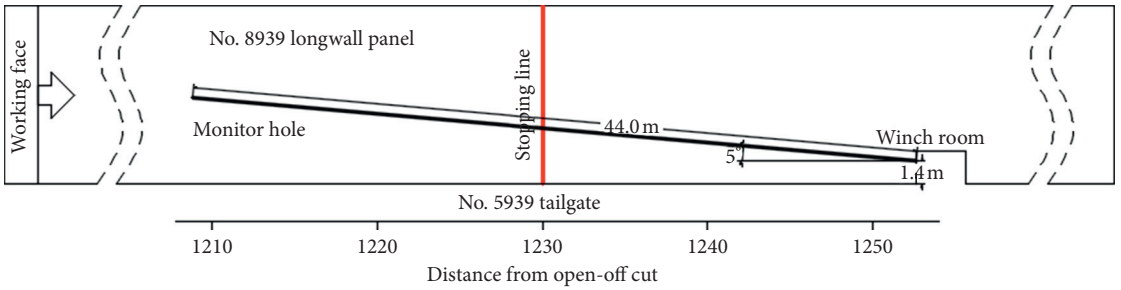

Figure 6: Plan view of optical fibre layout.

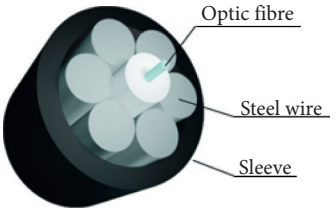

Figure 7: Internal structure of the optical cable.

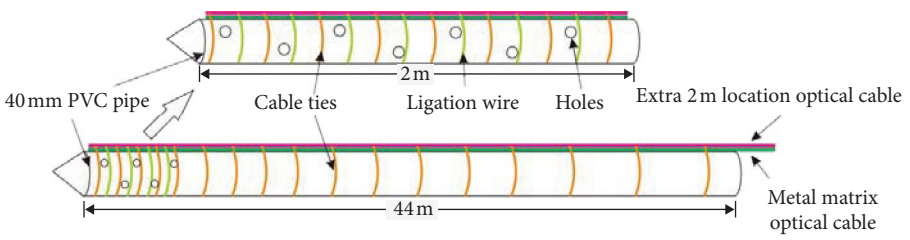

Figure 8: Schematic of distributed optical fibre sensor assembly in the field.

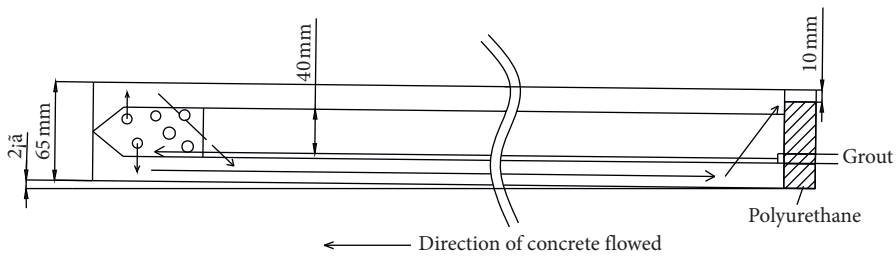

Figure 9: Schematic diagram of concrete pouring section.

Figure 10: The entire hole was grouted.

Figure 11: Optical time domain strain measurement instrument.

cable is connected to the BOTDR data acquisition instrument to collect the strain distribution along the whole optical cable. If the cable breaks at one point, the cable can be used up to the broken point. The errors due to the temperature change can be neglected as the variation is small in deep underground.

5. Analysis of Monitored Data Results

5.1. Data Analysis of Yielded Zone around Pressure Relief Boreholes of Different Diameters. Table 2 shows that the results of maximum strain and yielded zone radius for different borehole diameter. The average interval of 65 mm

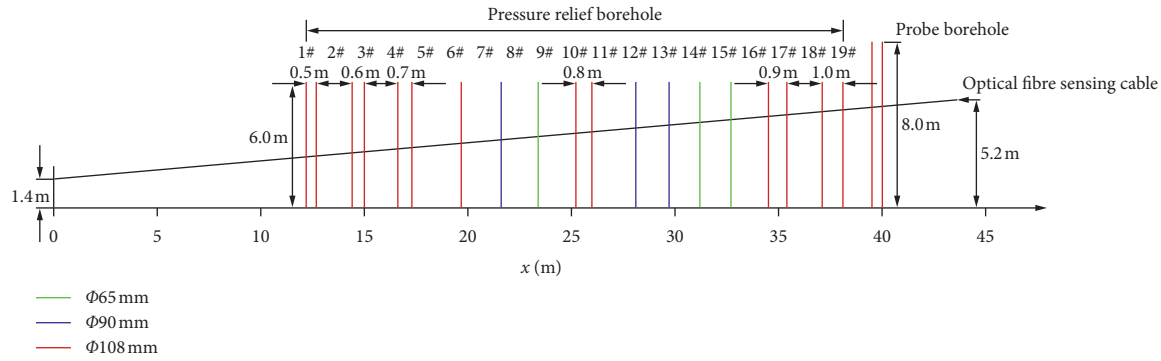

Figure 12: Plan view layout of pressure relief boreholes.

Table 2: Statistics of maximum strain and yielded zone radius for different borehole diameter.

Borehole diameter (mm)	65			Average	90			Average	108			Average
Borehole number	9#	14#	15#		8#	12#	13#		7#	10#	11#	
Maximum strain ($\mu\varepsilon$)	94	74	89	86	120	127	126	134	166	179	165	170
Yield radius (m)	0.36	0.32	0.35	0.34	0.44	0.49	0.44	0.46	0.71	0.74	0.68	0.71

diameter boreholes was about 1.5 m. The measured average maximum strain of the 65 mm pressure relief boreholes was 86 $\mu\varepsilon$, while the average pressure relief range was 0.34 m. For 90 mm pressure relief boreholes with an interval of 1.5–1.6 m, the maximum strain is 134 $\mu\varepsilon$, which is 55% higher compared with the measurement of the 65 mm boreholes. The average radius of pressure relief for 90 mm hole was 0.56 m, with a 65% increase compared with that of the 65 mm boreholes. The average maximum strain at the 108 mm borehole was measured to be 170 $\mu\varepsilon$, 98% higher than that of the 65 mm borehole. The average pressure relief range was 0.71 m, 108% higher compared with the 65 mm borehole. Thus, the 65 mm pressure relief borehole is not recommended for stress relief purpose.

Figure 13 shows that, with the increase of the borehole diameter, the strain zone around the borehole increases. It suggests that large diameter drilling hole should be used to minimize rock burst occurrences in coal mines.

5.2. Data Analysis of Yielded Zone around Pressure Relief Boreholes for Different Borehole Spacing. Twelve boreholes were divided into six groups (two boreholes in each group) to study the effect of the borehole interval. Two 108 mm boreholes were spaced at 0.5 m, 0.6 m, 0.7 m, 0.8 m, 0.9 m, and 1.0 m, as shown in Figure 9. It should be noted that all 108 mm boreholes yielded zone radii were about 0.7 m. The aim was to measure the maximum strain induced by drilling and the radius of the yielded zone around the two boreholes. In situ monitoring data are shown in Table 3. It shows that the pressure relief effects are similar, while the borehole spacing is less than 0.7 m. Strain versus borehole spacing is shown in Figure 14.

5.3. Data Analysis of Time-Dependent Pressure Relief around Boreholes. Table 4 and Figure 15 describe the influence of duration on pressure relief around the borehole. It should be noted that the accuracy of the optical cable is ±10 $\mu\varepsilon$. The measurements indicated that the strain changes were small just after drilling work. 288 hours after drilling, the strain increased to 108 $\mu\varepsilon$ and stabilized at a maximum of 134 $\mu\varepsilon$ after 432 hours. Data indicate that approximately 80% of strain occurs within 288 hours after drilling. Therefore, drilling should proceed at least 288–432 hours before mining operation to maximise the pressure relief in the coal seam.

To verify the optical fibre test results, a borehole peeper was used in the test. Take 10# borehole as an example. After 48 h of drilling, the borehole wall was smooth, as shown in Figure 16(a); after 168 h, some cracks occurred on the wall of the borehole, and there was fine cinder at the bottom of the borehole, as shown in Figure 16(b); after 240 h, internal part of the borehole collapsed, and there was broken lump coal at the bottom of the borehole, as shown in Figure 16(c); after 432 h, the borehole was completely collapsed, and the broken coal filled all free space, as shown in Figure 16(d).

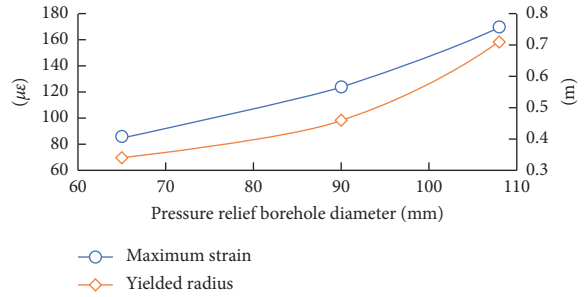

Figure 13: Strain change versus borehole diameter.

Table 3: Statistics of strain between two boreholes versus the borehole spacing.

Spacing of borehole (mm)	0.5	0.6	0.7	0.8	0.9	1.0
Diameter of borehole (mm)	108	108	108	108	108	108
Maximum strain ($\mu\varepsilon$)	157	142	123	24	−16	−22

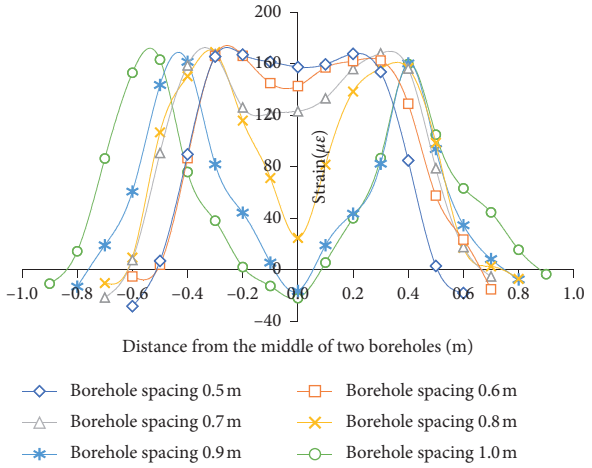

Figure 14: Strain versus borehole spacing.

Table 4: Statistics of strain versus time after drilling, borehole diameter, and spacing.

Testing time	24 h	72 h	168 h	240 h	288 h	360 h	432 h	480 h
Diameter of borehole (mm)	0.09	0.15	0.26	0.43	0.55	0.71	0.71	0.71
Maximum strain ($\mu\varepsilon$)	6	12	17	45	100	138	170	171

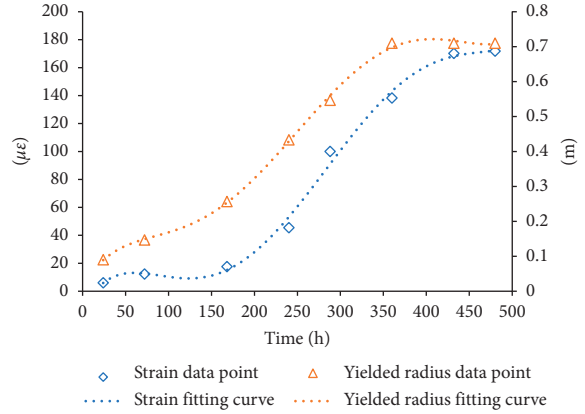

Figure 15: Strain versus time after drilling pressure relief boreholes.

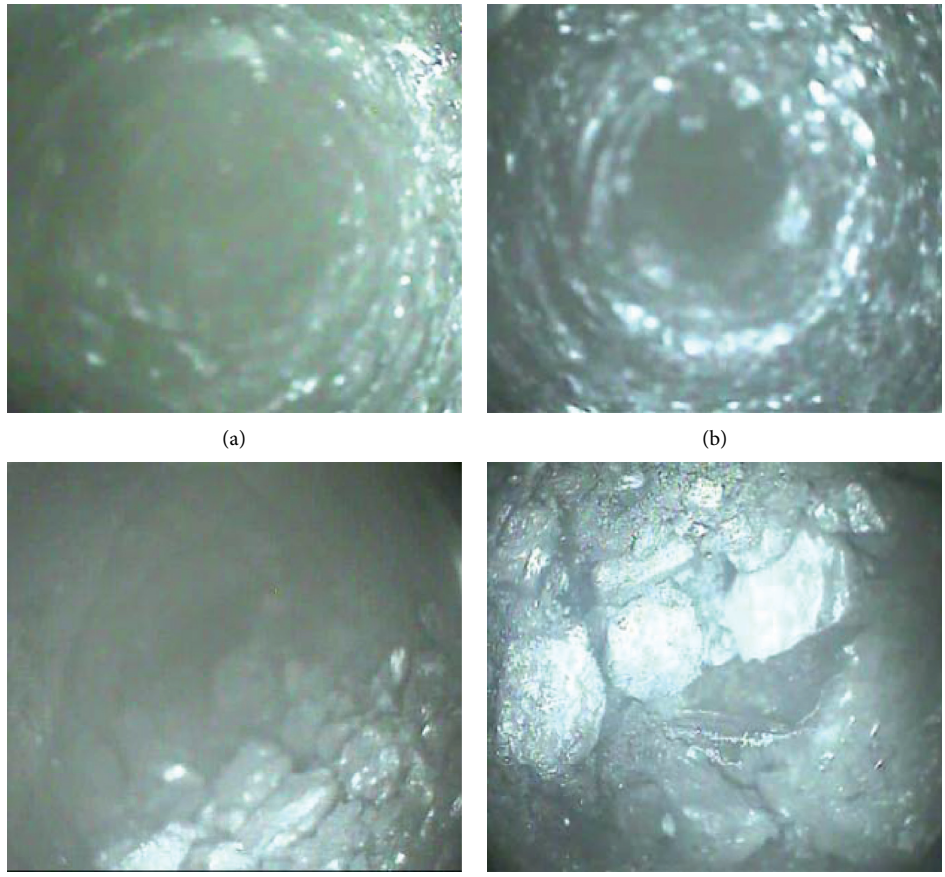

Figure 16: External test in 10# borehole: (a) drilled after 48 h, (b) drilled after 168 h, (c) drilled after 240 h, and (d) drilled after 432 h.

6. Conclusions

The proposed optical fibre sensing technology is a suitable method to determine the stress relief range around boreholes drilled in the coal seam.

(1) Based on the principle of borehole pressure relief and distributed optical fibre sensing technology, the internal strain sensing model of the coal body surrounding the pressure relief borehole is established.

(2) Through measurement of the strain around the pressure relief borehole, combined with the observation using related instrument, it is concluded that the process of the borehole collapse can be divided into initial stage, limit equilibrium stage, collapse stage, and compaction stage.

(3) The pressure relief borehole parameters suitable for the geological conditions of Xinzhouyao coal mine were determined.

(4) The optical fibre sensing technology is a novel approach to measure coal strain accurately. Results from this research provide new knowledge for mining practitioners to improve stress relief designs.

Data Availability

Most of the in situ test data generated by this work are shown in the manuscript, and other data can be obtained from the corresponding author upon request.

Conflicts of Interest

The authors declare that they have no conflicts of interest.

Acknowledgments

The authors gratefully acknowledge the support of the National Key Research and Development Program of China (nos. 2017YFC 0804201 and 2017YFC0804203) and Engineering Laboratory of Deep Mine Rockburst Disaster Assessment Open Project (LMYK2020004).

References

[1] Y.-D. Jiang and Y.-X. Zhao, "State of the art: investigation on mechanism, forecast and control of coal bumps in China," *Chinese Journal of Rock Mechanics and Engineering*, vol. 34, no. 11, pp. 2188–2204, 2015.

[2] Y.-D. Jiang, Y.-S. Pan, F.-X. Jiang, L.-M. Dou, and Y. Ju, "State of the art review on mechanism and prevention of coal bumps in China," *Journal of China Coal Society*, vol. 39, no. 2, pp. 205–213, 2014.

[3] R. Bernini, A. Minardo, and L. Zeni, "Reconstruction technique for stimulated Brillouin scattering distributed fibre-optic sensors," *Optical Engineering*, vol. 41, no. 9, pp. 186–194, 2002.

[4] B. Shen, O. Stephansson, and M. Rinne, "Simulation of borehole breakouts using Fracod2d," *Oil & Gas Science and Technology*, vol. 57, no. 5, pp. 579–590, 2002.

[5] T. H. Yang, T. Xu, H. Y. Liu, C. A. Tang, B. M. Shi, and Q. X. Yu, "Stress-damage-flow coupling model and its application to pressure relief coal bed methane in deep coal seam," *International Journal of Coal Geology*, vol. 86, no. 4, pp. 357–366, 2011.

[6] R. M. Khafizov, I. G. Khusainov, and V. S. Shagapov, "Dynamics of the pressure relaxation in a "depressurized" borehole," *Journal of Applied Mathematics and Mechanics*, vol. 73, no. 4, pp. 443–448, 2009.

[7] B. Lin, J. Zhang, C. Shen, Q. Zhang, and C. Sun, "Technology and application of pressure relief and permeability increase by jointly drilling and slotting coal," *International Journal of Mining Science and Technology*, vol. 22, no. 4, pp. 545–551, 2012.

[8] W. Meng, D.-J. Zheng, W.-L. Shen, X.-Y. Wang, and W.-F. Li, "Depressurizing boreholes for mitigating large deformation of the main entry," *Energy Science and Engineering*, vol. 8, pp. 1404–1417, 2019.

[9] P. Cui, B. Yao, Y. Liu, J. Wei, Z. Wen, and H. Li, "A new width measurement method of the stress relief zone on roadway surrounding rocks," *Geofluids*, vol. 8, pp. 1–12, 2019.

[10] S. Zhang, Y. Li, B. Shen, X. Sun, and L. Gao, "Effective evaluation of pressure relief drilling for reducing rock bursts and its application in underground coal mines," *International Journal of Rock Mechanics and Mining Sciences*, vol. 114, pp. 7–16, 2019.

[11] W.-L. Zhang, C. Li, J.-J Ren, and Z. Wu, "Measurement and application of vibration signals during pressure relief hole construction using microseismic system," *Measurement*, vol. 158, pp. 696–705, 2020.

[12] Z.-Q. Ma, Y.-D. Jiang, Y.-W. Li, and Y.-M. Yang, "Collaborative control of pressure released boreholes with U-steel of roadways in ultra-soft coal seam," *Journal of China Coal Society*, vol. 40, no. 10, pp. 2279–2286, 2015.

[13] M. K. Barnoski and S. M. Jensen, "Fiber waveguides: a novel technique for investigating attenuation characteristics," *Applied Optics*, vol. 15, no. 9, pp. 2112–2115, 1976.

[14] T. Horiguchi and M. Tateda, "BOTDA-nondestructive measurement of single-mode optical fiber attenuation characteristics using Brillouin interaction: theory," *Journal of Lightwave Technology*, vol. 7, no. 8, pp. 1170–1176, 1989.

[15] T. Horiguchi, K. Shimizu, T. Kurashima, M. Tateda, and Y. Koyamada, "Development of a distributed sensing technique using Brillouin scattering," *Journal of Lightwave Technology*, vol. 13, no. 7, pp. 1296–1302, 1995.

[16] R. Bernini, A. Minardo, and L. Zeni, "Distributed sensing at centimeter-scale spatial resolution by BOFDA: measurements and signal processing," *IEEE Photonics Journal*, vol. 4, no. 1, pp. 48–56, 2012.

[17] S. Nan and Q. Gao, "Application of distributed optical fiber sensor technology based on BOTDR in similar model test of backfill mining," *Procedia Earth and Planetary Science*, vol. 2, pp. 34–39, 2011.

[18] J. Xu, J. He, and L. Zhang, "Collapse prediction of karst sinkhole via distributed Brillouin optical fiber sensor," *Measurement*, vol. 100, pp. 68–71, 2017.

[19] W. Suo, Y. Lu, B. Shi, H. Zhu, G. Wei, and H. Jiang, "Development and application of a fixed-point fiber-optic sensing cable for ground fissure monitoring," *Journal of Civil Structural Health Monitoring*, vol. 6, no. 4, pp. 715–724, 2016.

[20] R. Moffat, J. Sotomayor, and J. F. Beltrán, "Estimating tunnel wall displacements using a simple sensor based on a Brillouin optical time domain reflectometer apparatus," *International Journal of Rock Mechanics and Mining Sciences*, vol. 75, pp. 233–243, 2015.

[21] B. Madjdabadi, B. Valley, M. B. Dusseault, and P. K. Kaiser, "Experimental evaluation of a distributed Brillouin sensing system for detection of relative movement of rock blocks in underground mining," *International Journal of Rock Mechanics and Mining Sciences*, vol. 93, pp. 138–151, 2017.

[22] A.-Q. Li, Y.-S. Song, B. Zhang, Y. Liu, and N.-S. Yu, "Experimental study on strain and deformation monitoring of reinforced concrete structures using PPP-BOTDA," *Science in China Series E: Technological Sciences*, vol. 52, no. 10, pp. 2859–2868, 2009.

[23] A. Klar, I. Dromy, and R. Linker, "Monitoring tunneling induced ground displacements using distributed fiber-optic sensing," *Tunnelling and Underground Space Technology*, vol. 40, pp. 141–150, 2014.

[24] C.-Y. Hong, Y. F. Zhang, G.-W. Li, M.-X. Zhang, and Z.-X. Liu, "Recent progress of using Brillouin distributed fiber optic sensors for geotechnical health monitoring," *Sensors and Actuators A: Physical*, vol. 258, pp. 131–145, 2017.